

# Three-dimensional ground displacements from static pipe bursting in stiff clay

R.W.I. Brachman, H.A. McLeod, I.D. Moore, and W.A. Take

**Abstract:** Three-dimensional ground surface displacements from 20 m long static pipe-bursting experiments are reported. These experiments were conducted with firm-to-stiff clay backfill in a trench with very stiff clay sidewalls at three different burial depths. Multiple digital cameras and image analysis were used to quantify the surface response as the expander progressed through the original pipe. The experiments quantified the upward surface movement as the expander approached, the effect of burial depth on maximum uplift, and the final amount of uplift after it decreased to a residual displacement. The experiments also quantified the axially forward ground surface movement as the expander approached, reaching maximum just ahead of the expander, and decreasing to almost zero after the expander had passed by. Lateral movements of the ground surface away from the centreline are also reported, which were essentially zero at the centre line, increasing to a maximum and then decreasing with distance from the centreline. The three different burial depths produced in effect the same width of vertical surface response with the displacements contained within 1.5 m on either side of the centreline, suggesting that the very stiff clay trench walls had a dominant influence on the measured displacements.

*Key words:* static pipe bursting, ground displacements, trenchless technology.

**Résumé :** Des déplacements en trois dimensions de la surface d'un sol provenant d'essais d'éclatement d'un tuyau statique de 20 m de long sont présentés. Ces essais ont été effectués dans une tranchée remblayée avec de l'argile ferme à rigide avec des murs latéraux faits d'argile très rigide, et ce à trois profondeurs d'enfouissement différentes. Plusieurs caméras digitales et de l'analyse d'image ont été utilisées afin de quantifier les mouvements de surface vers le haut pendant le déplacement de l'extenseur, l'effet de la profondeur d'enfouissement sur le soulèvement maximal, ainsi que le soulèvement final après la diminution jusqu'à la valeur de déplacement résiduel. Les essais ont aussi permis de quantifier le mouvement axial de la surface du sol vers l'avant à l'approche de l'extenseur, ce mouvement atteignant un maximum juste avant l'extenseur, et diminuant à près de zéro après que l'extenseur soit passé. Les mouvements latéraux de la surface du sol vers l'extérieur de la ligne centrale sont aussi présentés. Ceux-ci sont essentiellement de zéro sur la ligne centrale, ensuite augmentant jusqu'à un maximum suivi par une diminution avec une plus grande distance de la ligne centrale. Les trois profondeurs d'enfouissement différentes ont produit des mouvements de surface verticaux ayant sensiblement la même largeur, avec des déplacements contenus dans les 1,5 m de chaque côté de la ligne centrale, ce qui suggère que les murs latéraux d'argile très rigide ont une influence dominante sur les déplacements mesurés.

*Mots-clés :* éclatement d'un tuyau statique, déplacements de sol, technologie sans tranchée.

[Traduit par la Rédaction]

## Introduction

Static pipe bursting is a trenchless construction technique where an existing pipe that is hydraulically or structurally deficient is replaced with a new pipe without the need for extensive surface disruption associated with conventional cut-and-cover pipe replacement. As shown in Figs. 1 and 2, pipe bursting involves pulling an expander through the original pipe to break it apart and enlarge the soil cavity. The new pipe is attached to the rear of the expander and is pulled into place directly after the fragments of the old pipe are pushed aside. The magnitude and distribution of ground

surface displacements induced from static pipe bursting (as opposed to pneumatic pipe bursting) are the focus of this paper.

Surface displacements may depend on the displacement imposed by the expander on the original pipe, the response of the surrounding ground within a zone of influence, and geometrical factors such as burial depth and trench width. In terms of the first component, the vertical displacement imposed on the inside crown of the original pipe is related to the difference between the diameter of the expander ( $D$ ) and the inside diameter of the original pipe ( $ID_o$ ) and also the trajectory of the expander relative to the original pipe. For example, if the expander remains concentric with the original pipe, then the vertical displacement imposed on the inside crown of the original pipe is equal to one-half of the difference between  $D$  and  $ID_o$ ; whereas, if the base of the expander traverses along a plane corresponding to the initial elevation of the invert of the original pipe (i.e., no downward displacement of the invert of the pipe), then the upward vertical displacement imposed at the crown of the original pipe would be twice as large and equal to  $D - ID_o$ .

Received 13 July 2009. Accepted 1 October 2009. Published on the NRC Research Press Web site at [cgj.nrc.ca](http://cgj.nrc.ca) on 2 April 2010.

**R.W.I. Brachman,<sup>1</sup> I.D. Moore, and W.A. Take.**

GeoEngineering Centre at Queen's-RMC, Queen's University, Kingston, ON K7L 3N6, Canada.

**H.A. McLeod.** Golder Associates Ltd., 220 – 1755 Springfield Road, Kelowna, BC V1Y 5V5, Canada.

<sup>1</sup>Corresponding author (e-mail: [Brachman@civil.queensu.ca](mailto:Brachman@civil.queensu.ca)).

**Fig. 1.** Transverse cross section illustrating (a) initial conditions and (b) surface displacement from pipe bursting.

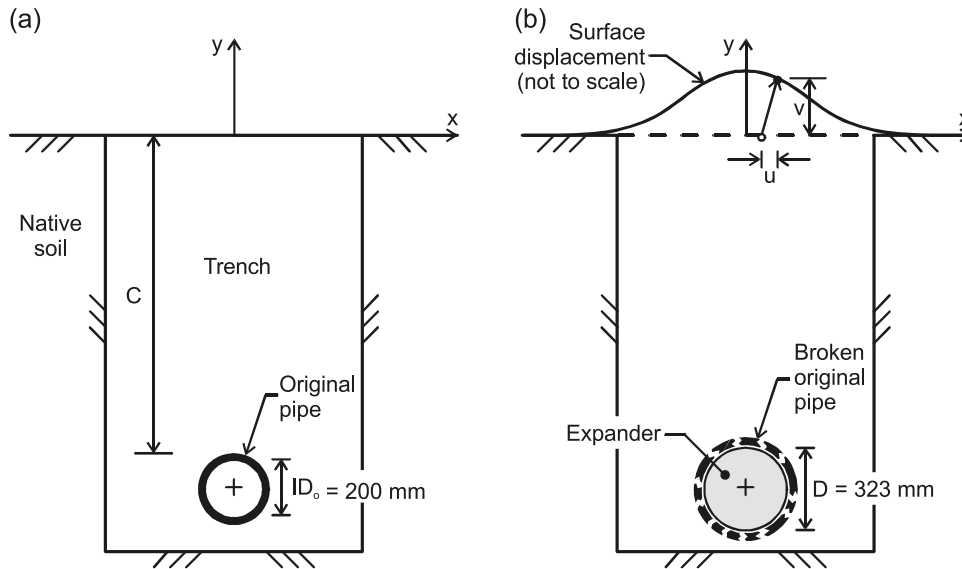
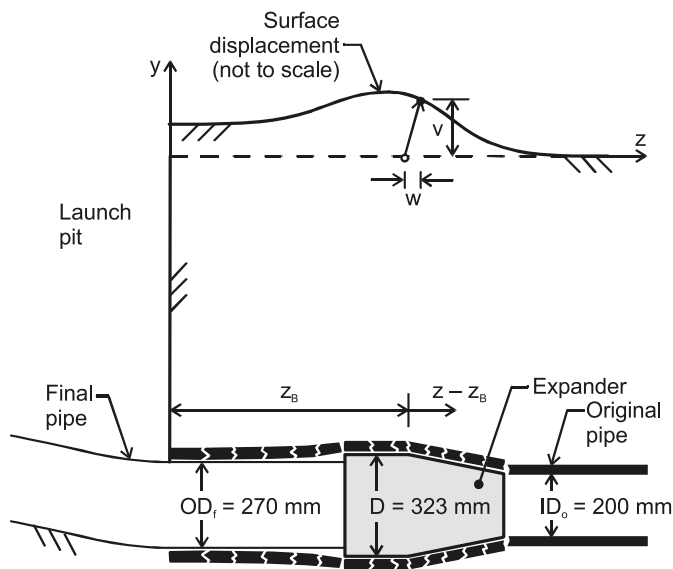


**Fig. 2.** Axial cross section illustrating surface displacements induced from pipe bursting.



What actually happens to the original pipe may depend on the compressibility and strength of the ground above and below the pipe and the burial depth (e.g., see Fernando 2002). The surrounding ground is expected to undergo shear failure (e.g., see Nkemitag and Moore 2007) and thus, larger surface displacements would be expected with dilative materials (e.g., dense coarse-grained materials) than with materials that experience little or no volume strain upon shear failure (e.g., saturated fine-grained soil under rapid loading). As for geometry, one would expect smaller displacements as the burial depth increases, as the displacements would be attenuated over a larger volume of soil.

There is a growing database of ground displacement measurements from static pipe bursting. For example, field tests reported by Atalah et al. (1998) in clay, laboratory tests by Rogers and Chapman (1995) and Lapos (2004) in poorly

graded sand, and tests by Cholewa et al. (2009) in well-graded sand and gravel. However, no detailed three-dimensional surface displacement measurements are available for pipe bursting in stiff clay over a range of burial depths.

Results from three 20 m long static pipe-bursting experiments are reported in this paper. These experiments were conducted with firm-to-stiff clay backfill in a trench with very stiff clay sidewalls at different burial depths. The objectives are to (i) quantify the magnitude and distribution of the three-dimensional surface displacements, (ii) assess the influence of burial depth on surface displacements, and (iii) compare the new measurements to existing results to gain additional insights into ground displacements induced by static pipe bursting.

## Method

### Experimental details

Three 20 m long pipe-bursting experiments were conducted. For reference,  $x$  is transverse to the pipe centreline with  $x = 0$  at the pipe centreline as shown in Fig. 1, while  $z$  is in the axial direction along the pipe with  $z = 0$  taken at the launch pit as shown in Fig. 2. The distance along the pipe axis from the expander to the launch pit is defined as  $z_B$  (Fig. 2).

The expander had a minimum diameter of 200 mm at its leading edge, then a 300 mm long truncated cone segment that transitioned into a 200 mm long cylinder with a diameter ( $D$ ) of 323 mm. The original pipe in these experiments was a new vitrified clay pipe with an inside diameter ( $ID_o$ ) of 200 mm and an outside diameter of 250 mm. A high-density polyethylene (HDPE) pipe having an inside diameter of 234 mm and an outside diameter ( $OD_i$ ) of 269 mm was pulled into place behind the expander to serve as the new pipe in these experiments.

Three burial depths were tested: 0.6, 1, and 1.5 m of cover ( $C$ ) from the outside crown of the original pipe to the ground surface. These are denoted as tests 1 to 3, respectively. The clay pipes were installed in trenches cut into the

very stiff native clay. The dimensions of the trenches (averaged from measurements at three points along their 20 m length) are given in Fig. 3. All three trenches were approximately 0.8 m wide at the bottom, but the width at the ground surface increased as the trench depth increased. Once the trench was excavated, a bedding layer of crushed gravel was placed followed by installation of the pipe. The trench was backfilled with crushed gravel up to the crown of the pipe (placed at an average dry density of  $1580 \pm 50 \text{ kg/m}^3$ ) and then native clay material was used to backfill the trench to the ground surface. The backfill was placed in approximately 0.3 m thick lifts and was compacted using the bucket of an excavator. Great effort was made to break any clods in the clay, which was believed to be successful, as there was no evidence of interclod macrovoids in the clay backfill from post-test exhumations. The pipes were installed between 12 and 15 December 2007.

The pipe-bursting experiments were conducted between 22 and 26 August 2008. The difference in time between pipe installation and pipe bursting allowed the trench backfill to settle and come into moisture equilibrium with its new boundary conditions. The bursting started from the launch pit at  $z = 0$  and advanced through the pipe towards the retrieval pit at  $z = 20$  m. A hydraulically powered Grundoburst 800G system with a maximum machine pressure of 25 MPa was used for the pipe-bursting process. The actual machine pressure required to pull the expander and new pipe into place was less than 8 MPa.

### Ground conditions

The ground conditions were examined by (i) taking grab samples from the trench walls during excavation for liquid ( $w_L$ ) and plastic ( $w_P$ ) limit testing, (ii) measuring the volumetric water content ( $\theta_v$ ) using time domain reflectometry along the trench walls and in the trench backfill immediately after each test, and (iii) conducting cone penetration tests that provided the continuous measurements of tip resistance ( $q_c$ ), friction ratio ( $R_f$ ), and undrained shear strength ( $S_u$ ) with depth in the trench backfill and native material for test 3. A summary of results are plotted in Figs. 4–6. The particular details for each test method can be found in McLeod (2008).

The uppermost 0.3–0.6 m layer of native soil was stiff organic clay of high plasticity (clayey silt to silty clay with variable sand and gravel content). This is evident in Fig. 4 by the higher liquid limit closer to the surface and is consistent with past agricultural use of the site. Deeper, there was very stiff silty clay to clayey silt of low plasticity. The index limits in Fig. 4 are similar with depth, indicating that the ground conditions did not vary significantly between the three experiments.

Figure 5 shows that the volumetric water contents in the native and backfill soil were similar to a depth of 0.7 m at the time of testing. All three tests showed a trend towards a drier crust zone within the first 0.3 m below the ground surface. Below 0.5 m, the volumetric water content was 30  $\pm$  5%, which is close to saturation for this very stiff material.

The cone penetration results in Fig. 6 show a stronger crust to a depth of about 0.5 m for both the native and backfill soils with an undrained shear strength greater than 100 kPa. Between 0.5 and 1.5 m, the tip resistance was

lower and the friction was higher in the backfill soil, indicating that the backfill was not as strong or as stiff as the native soil. The undrained shear strength of the native soil was around 100 kPa, while for the backfill it varied between 30 and 80 kPa.

### Surface displacement measurement

The three-dimensional surface displacements were obtained by first capturing successive digital images of surface targets throughout each experiment and then using particle image velocimetry (e.g., White et al. 2003) to analyze those images to compute the displacements. Figure 7 is a plan view of the experiment showing the location of five digital cameras. Cameras 1–4 were positioned transverse to the pipe (looking in the  $x$ -direction) to capture vertical and axial surface displacements. These cameras were located 13 m from the centreline of the pipe, well outside of the zone of ground movement. Camera 5 was placed beside the receiving pit looking along the length of the pipe (in the  $z$ -direction) to capture vertical and horizontal surface displacements. A sixth camera was positioned facing the launch pit to track the movement of the new pipe.

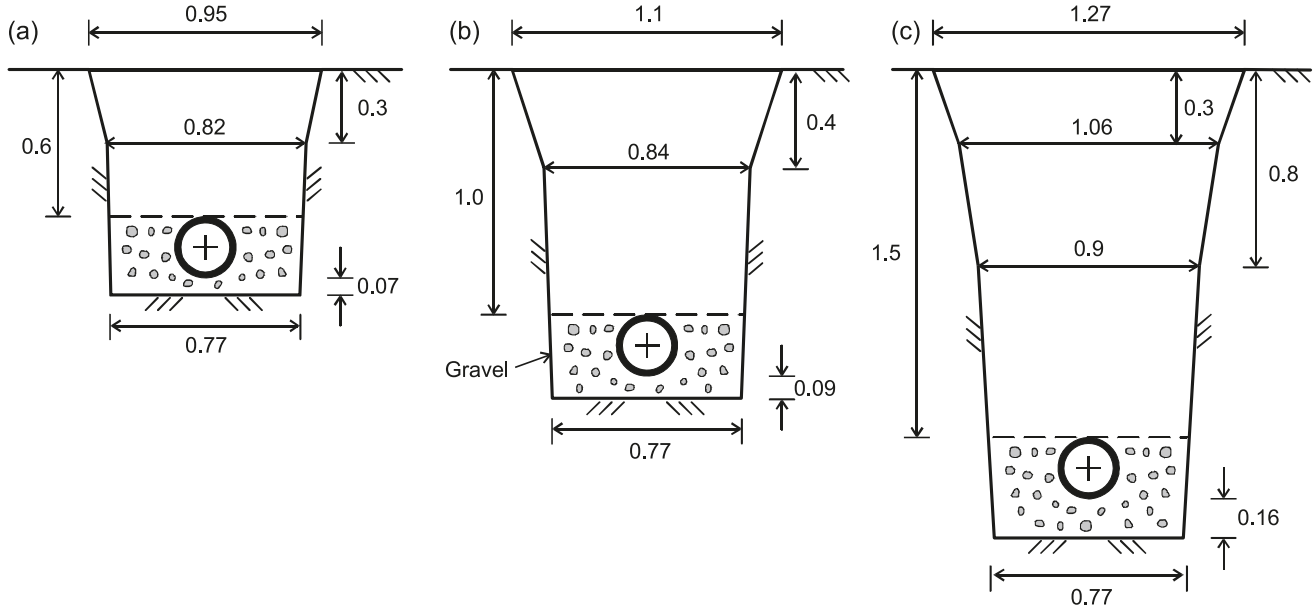
The targets consisted of 38 mm  $\times$  38 mm  $\times$  38 mm wood blocks with each vertical face painted white and having a 25 mm black character located approximately in the centre. A total of 409 surface targets were placed between  $2 < z < 18$  m along the length of the pipe and  $-4 < x < 4$  m transverse to the pipe, as shown in Fig. 7. Reference boards (0.6 m by 0.9 m targets) placed in line with each camera, but outside of the zone of influence, were used to correct for potential errors arising from camera movement or changes in lighting. Figure 8 is an image obtained from camera 3 and shows the targets, reference board, and cameras 2 and 4.

Prior to each experiment, 20 images were taken and these were averaged to obtain the initial conditions. Then during the pipe-bursting process, as the expander advanced approximately 0.75 m (to remove a 0.75 m long segment of pulling rod), 10 images of the ground surface were taken. This process was repeated until bursting was completed, then another series of 20 images was taken to capture the residual movement. By taking multiple images at each expander location, the potential error was reduced. The potential error associated with these surface measurements has been shown to be less than  $\pm 0.1$  mm (McLeod 2008).

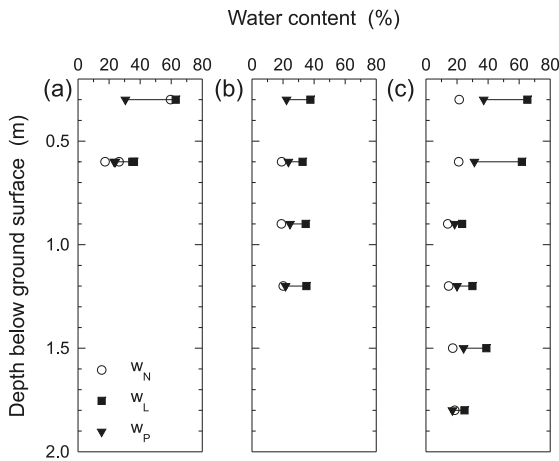
### Results

Figure 9 shows a sequence of vertical surface displacement,  $v$  (as defined in Figs. 1 and 2), contours from test 2 ( $C = 1$  m) as the expander advanced through the original pipe. As expected, the pipe-bursting operation induced a three-dimensional response of the ground surface. For example, Fig. 9a shows the displacements when the axial position of the expander was at  $z = 6$  (i.e.,  $z_B = 6$  m). At this point in the experiment, surface displacements extended 1.5 m in advance of the expander and approximately 1.5 m in the transverse direction on either side of the expander. The progression of surface displacements in advance of the expander for  $z_B$  between 6 and 15 m are very similar, as shown in Figs. 9a–9d. Vertical displacements at any given

**Fig. 3.** Trench geometry for tests (a) 1, (b) 2, and (c) 3. All dimensions in m.



**Fig. 4.** Liquid ( $w_L$ ) and plastic ( $w_P$ ) limits and natural gravimetric water content ( $w_N$ ) from grab samples along trench wall for tests (a) 1, (b) 2, and (c) 3. Data obtained in December 2007.



**Fig. 5.** Volumetric water content ( $\theta_v$ ) for native and backfill soil for tests (a) 1, (b) 2, and (c) 3. Data obtained immediately after testing in August 2008.

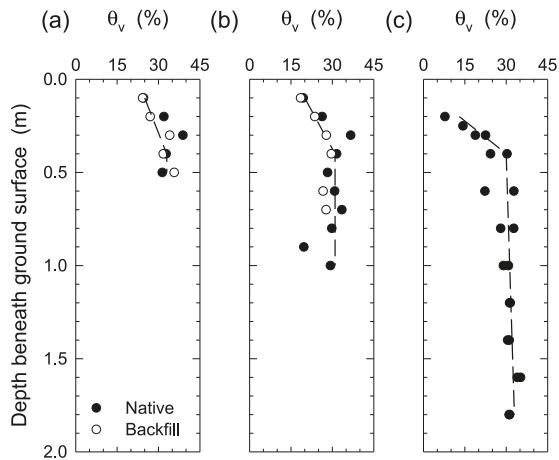
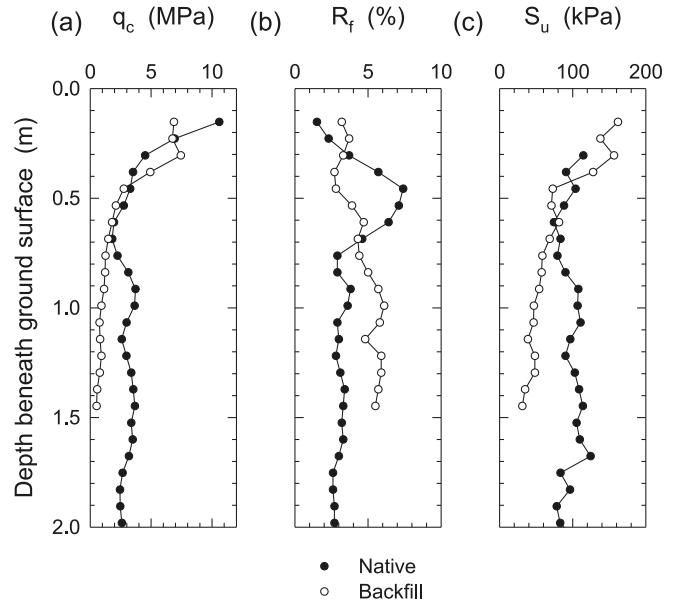


**Fig. 6.** Cone penetration test results for test 3: (a) cone tip resistance, (b) friction ratio (ratio of sleeve to tip resistance), and (c) undrained shear strength. Data obtained immediately after testing in August 2008.



axial position increased to a maximum value as the expander passed beneath that location and then decreased to a residual displacement as the expander continued to advance through the original pipe. Similar patterns of surface displacement, albeit with differing magnitudes, were found for tests 1 and 3 and their surface contours have been reported by McLeod (2008).

The largest values of vertical displacement measured for each point along  $x = 0$  from tests 1 to 3 are plotted in Fig. 10. It is evident in this figure that the magnitude of vertical displacement decreased as the cover depth increased from 0.6 m in test 1 to 1.5 m in test 3. These results also reveal the level of variability in the measurements for each

**Fig. 7.** Plan view showing setup for surface displacement measurements.

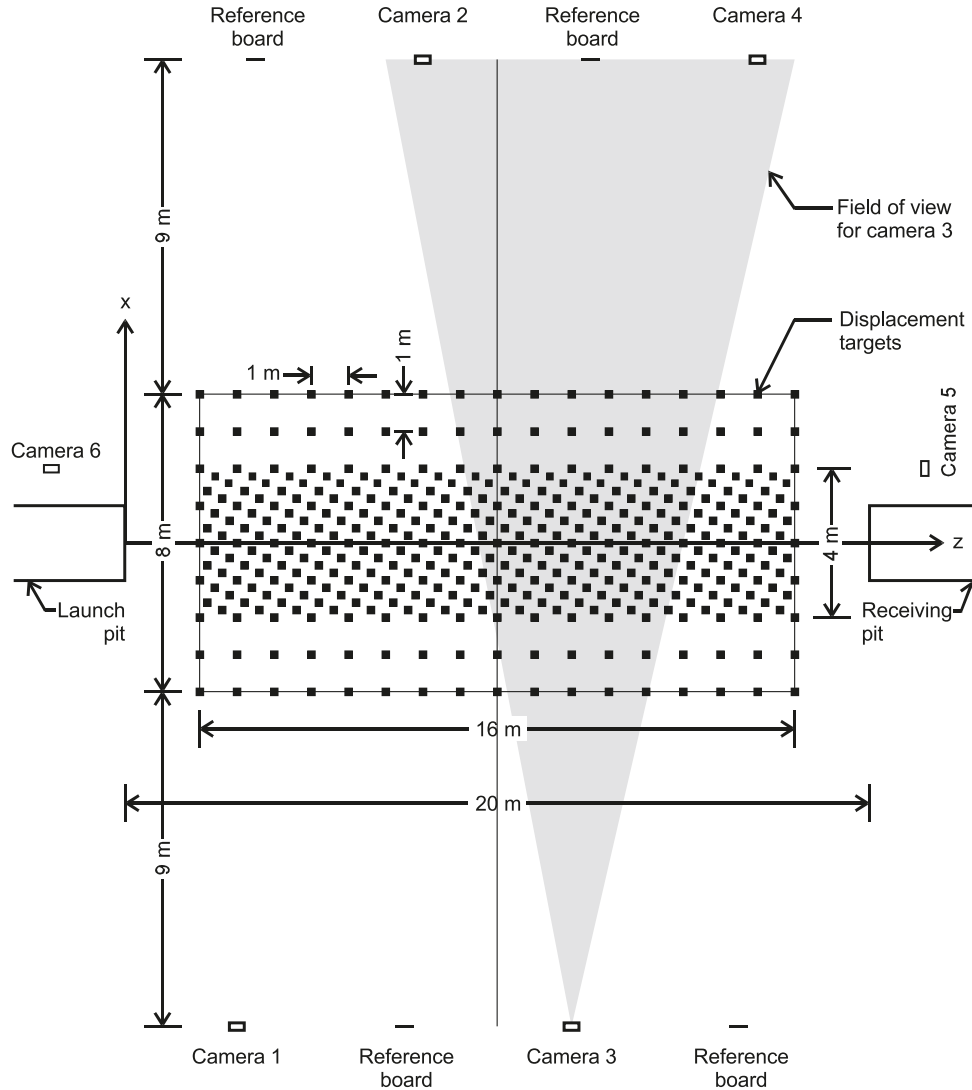
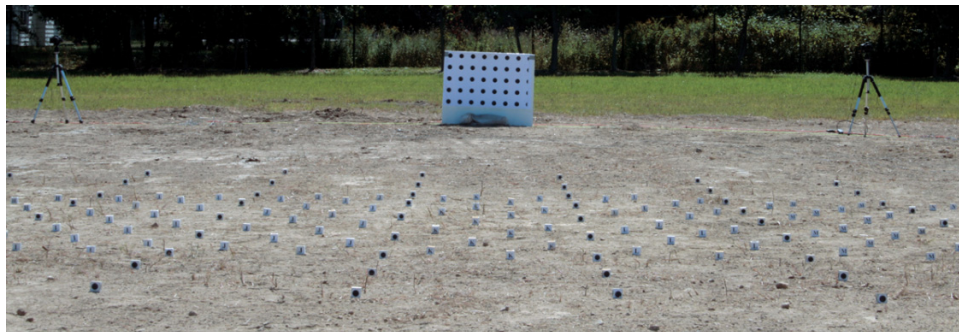


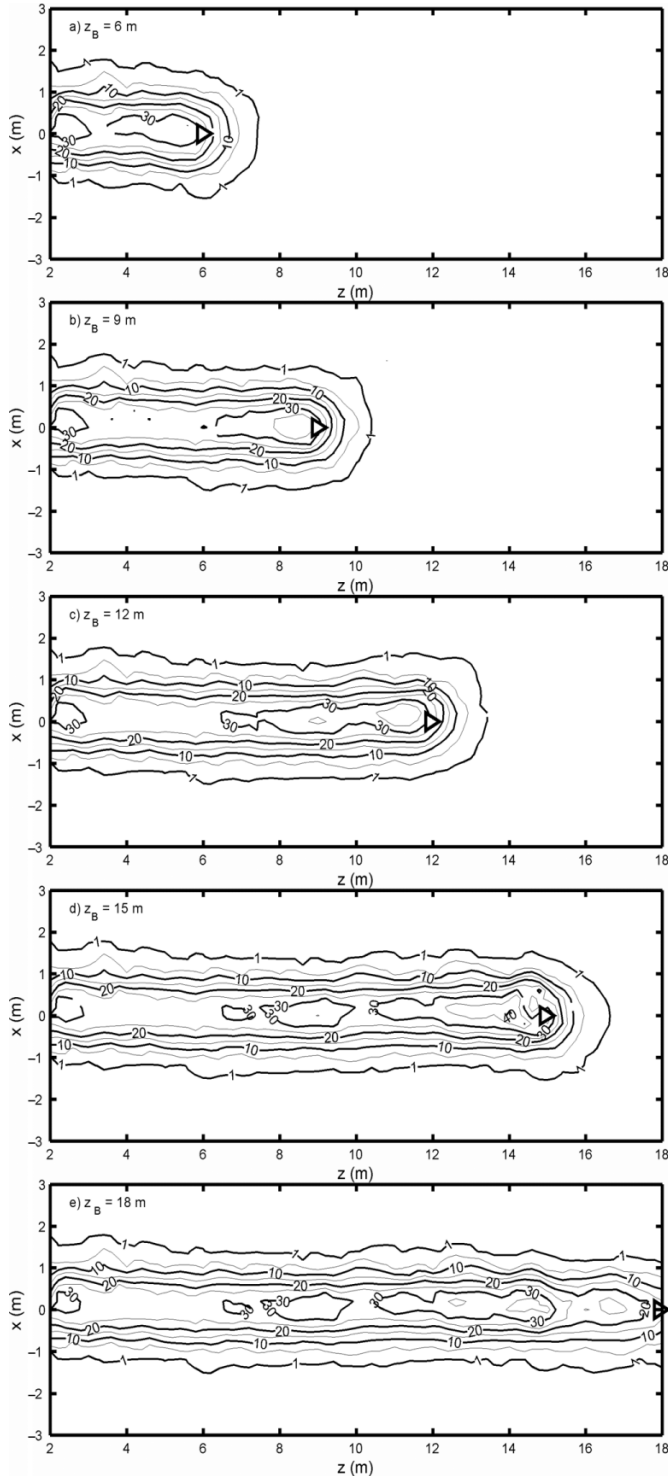
**Fig. 8.** Photograph from camera 3 looking transverse to pipe centreline showing surface displacement target blocks, reference board, and cameras 2 and 4.



test. Figure 10 shows no discernable influence of the launch and retrieval pits on the results from test 1. Test 2 shows an abrupt decrease towards the retrieval pit for  $z > 17$  m. This coincides with a 1 m long segment of the original pipe being dislodged into the open retrieval pit near the end of bursting, which likely produced an unsupported cavity at the former

position of the original pipe that may have influenced the ground displacements in this region. For test 3, the launch pit appears to influence surface displacements, as there is a noticeable steady increase in displacement for  $z < 5$  m. Therefore, to remove bias from potential end effects of the launch and retrieval pits, data from the central 10 m (i.e.,

**Fig. 9.** Contours of vertical surface displacement (mm) as the expander (indicated by the triangle) advanced for test 2, showing  $z_B =$  (a) 6 m; (b) 9 m; (c) 12 m; (d) 15 m; (e) 18 m.



$5 < z_B < 15$  m) was subsequently used to produce representative sections for each experiment.

Apart from potential end effects, the variations in Fig. 10 are attributed to the inherent variability in backfill ground conditions and fragmenting of the original clay pipe. For

**Fig. 10.** Largest vertical displacement measured for each point along  $x = 0$ .

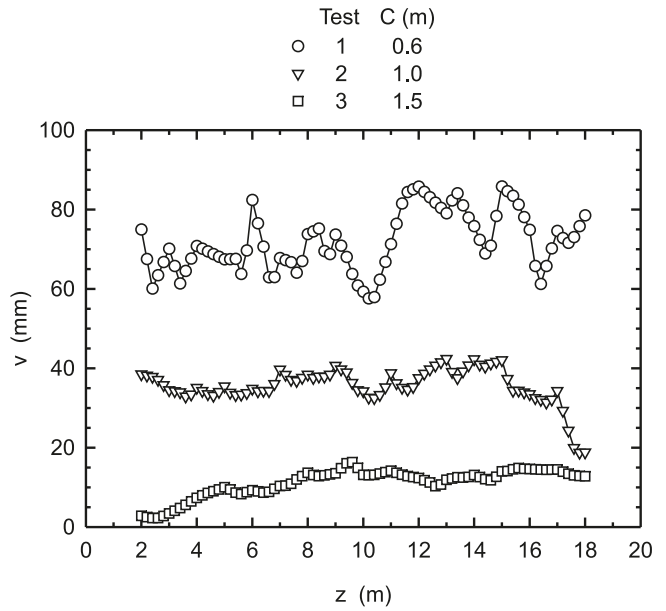


**Fig. 11.** Vertical displacement along  $x = 0$  relative to location of expander ( $z_B$ ) showing mean and standard deviation for  $5 < z_B < 15$  m.

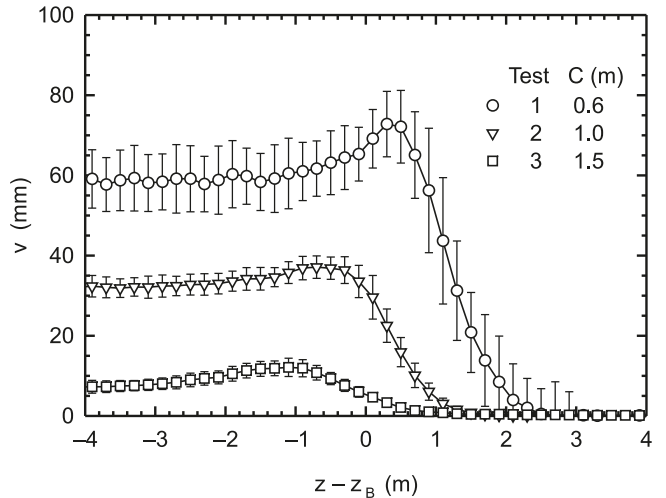


**Fig. 12.** Maximum vertical displacements showing mean and standard deviation for  $5 < z_B < 15$  m.

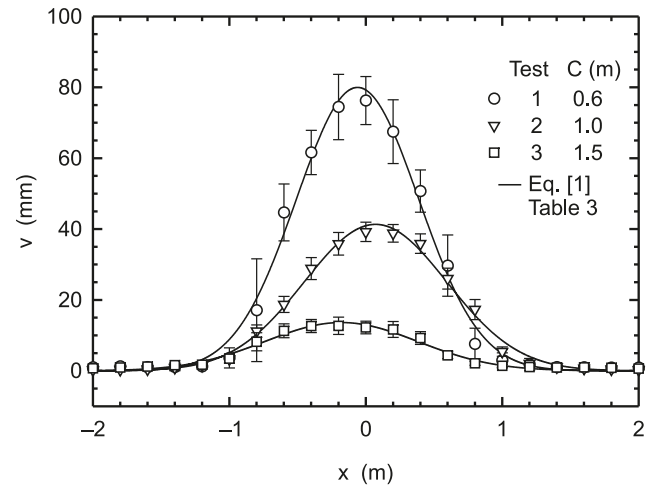


**Table 1.** Measured peak ground surface displacements.

Test	Cover (m)	Vertical displacement			Axial displacement			Horizontal displacement		
		Mean (mm)	Standard deviation (mm)	$z - z_B$ (m)	Mean (mm)	Standard deviation (mm)	$z - z_B$ (m)	Mean (mm)	Standard deviation (mm)	$x$ (m)
1	0.6	76	7	0.3	12	3	1.3	10	3	0.4
2	1.0	39	3	-0.7	8	1	0.3	7	1	0.8
3	1.5	13	2	-1.1	2	1	-0.1	3	0.4	0.4

the shallower cover in test 1 ( $C = 0.6$  m), the displacements were more variable than the other two tests. This greater variation occurred because the expander was so close to the surface that there was less overlying soil to help attenuate local effects such as those from individual fragments of the original pipe. For the deepest burial condition in test 3 ( $C = 1.5$  m), the surface movement appears to be less sensitive to variations in pipe breakage and soil strength and stiffness.

Figure 11 shows the axial progression of the vertical surface displacements relative to the position of the expander. This was obtained by subtracting the location of the expander ( $z_B$ ) from the location of the measurements ( $z$ ), and the values shown represent the average of 13 data sets gathered for  $5 < z_B < 15$  m along  $x = 0$ . For example,  $z - z_B = 0$  corresponds to a position directly above the largest diameter of the expander (e.g., see Fig. 2). In each test, the vertical displacement increased sharply to the maximum value but then approached the residual surface displacement more gradually after the expander had passed overhead. The location of maximum displacement relative to the expander changed from a position 0.3 m ahead to a position 1.1 m behind the expander as the cover depth increased from 0.6 m in test 1 to 1.5 m in test 3. The distance ahead of the expander where vertical displacements first became noticeable decreased from 2.3 m (when  $C = 0.6$  m) to 0.5 m (when  $C = 1.5$  m).

Figure 12 shows a transverse section of the maximum vertical displacements when averaged for the 30 data sets between  $5 < z_B < 15$  m. The pattern of displacement is symmetric and just slightly ( $<0.1$  m) off centre for tests 1 and 2, and 0.2 m off centre for test 3. Peak vertical displacements for the three tests are given in Table 1. The vertical displacements were largely contained within a distance 1.5 m on either side of the centreline for all three tests.

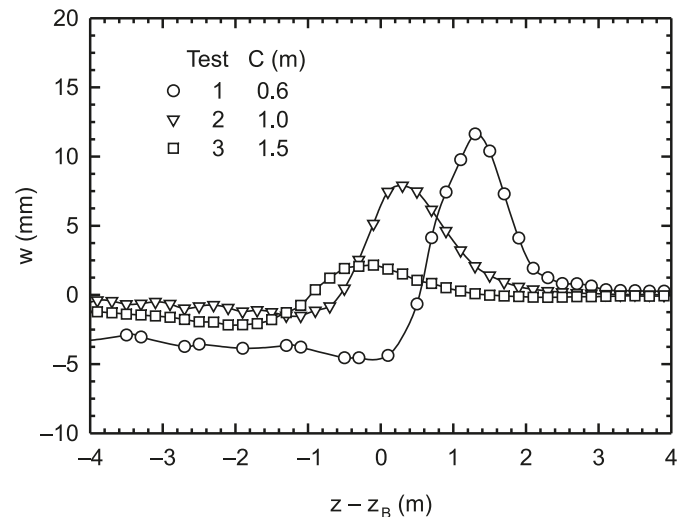
Residual vertical displacements were measured once the expander was extracted into the recovery trench. The average residual vertical displacements between  $5 < z < 15$  m for the three tests are given in Table 2.

The progression of axial surface displacements,  $w$  (as defined in Fig. 2), relative to the position of the expander along  $x = 0$  are plotted in Fig. 13. Points on the ground surface experienced a forward axial displacement as the expander approached and passed beneath them and then displaced axially backwards as the expander advanced further. The peak axial displacements are given in Table 1. As seen for the vertical displacements, smaller cover resulted in larger axial displacements. The pattern of surface axial displacements is better illustrated in Fig. 14, which shows the average vertical and axial displacement trajectory followed by points along  $x = 0$ . For all tests, the surface moved vertically upwards and axially forward, then axially backwards

**Table 2.** Measured residual vertical displacements along  $x = 0$ .

Test	Cover (m)	Vertical displacement (mm)	
		Mean	Standard deviation
1	0.6	58	7
2	1.0	31	3
3	1.5	6	1

**Fig. 13.** Axial displacement along  $x = 0$  relative to location of expander ( $z_B$ ) showing mean for  $5 < z_B < 15$  m.



as it continued to move vertically upwards, and finally downward to the residual vertical displacement and slightly axially forward to a residual axial displacement of zero essentially. Figure 14 also shows that the magnitudes of axial displacements are about one-sixth of the vertical displacements.

The maximum horizontal surface displacements,  $u$  (as defined in Fig. 1), are given in Fig. 15 and the peak displacements are summarized in Table 1. In Fig. 15, a positive displacement corresponds to a point being moved horizontally away from the centreline ( $x = 0$ ). For each test, horizontal displacements increased to a maximum and then decreased further away from the centreline. This mode of deformation implies that the centreline experiences horizontal tensile elongation. Surface cracks aligned in the axial direction were observed after tests 1 and 2 and are consistent with the measured mode of horizontal displacement.

**Fig. 14.** Vertical and axial displacement trajectory of surface at  $x = 0$  for  $2 > (z - z_B) > -2$ . Solid data points every  $\pm 0.2$  m from  $(z - z_B) = 0.1$  m.

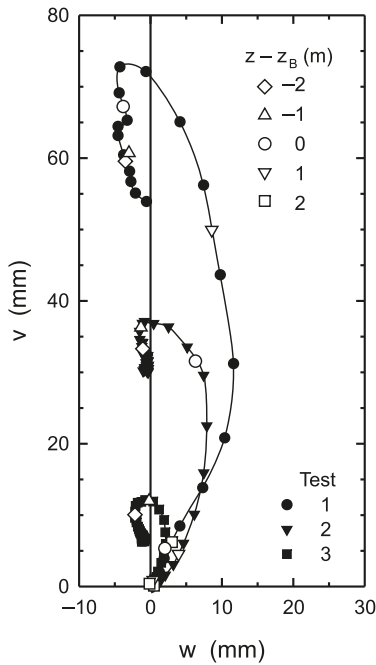
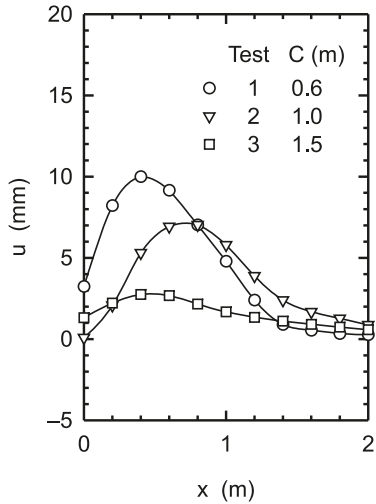


**Fig. 15.** Maximum horizontal displacements.



**Discussion**

The three-dimensional response of the ground surface was effectively captured using multiple digital cameras and image analysis. This enabled simultaneous displacement measurements at 409 surface locations for over 20 positions of the expander during each test. Once quantified, it is evident that the location of the maximum with respect to the position of the expander is not necessarily known at the start of the experiment and may vary between experiments (e.g., see Fig. 11). Thus, for such experiments, it is important to have multiple, closely spaced measurements, especially for shallow cover where the displacements are much larger and more variable than those for deeper cover.

**Fig. 16.** Measured surface displacements versus depth of cover.

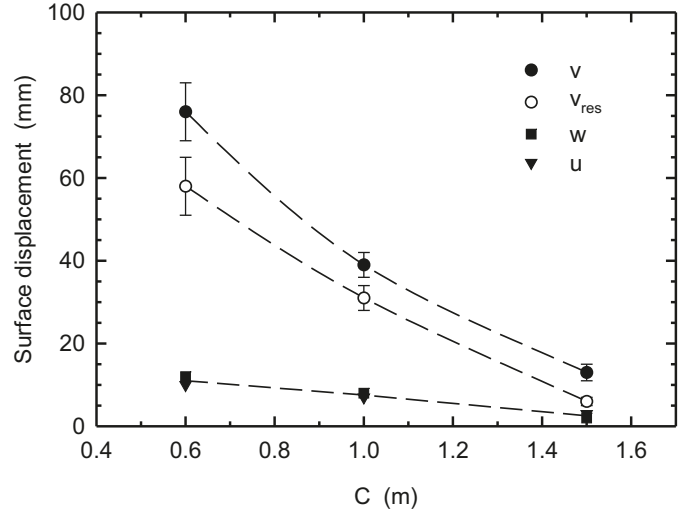


**Table 3.** Gaussian fit to vertical displacements.

Test	Cover (m)	$v_p$ (mm)	$i$ (m)	$x_0$ (m)	$R^2$
1	0.6	80	0.45	-0.06	0.991
2	1.0	41	0.53	0.07	0.993
3	1.5	13	0.53	-0.18	0.980

As expected, the measurements of surface displacement in all three directions (vertical, axial, and horizontal) increased with decreasing burial depth. The trend with cover depth is plotted in Fig. 16. Thus, for most practical pipe burial depths in Canadian and other cold climates where pipe burial is often at a minimum of 1.5 m deep to control frost effects, very small surface displacements (<15 mm) can be expected for the ground and pipe replacement conditions tested. While the shallow cover of 0.6 m led to the largest surface displacements, it may have limited direct practical application for these environments, but nonetheless provides a useful upper bound for these conditions and will have more practical significance where pipes can be buried at shallower depths.

Plotted in Fig. 12 along with the measured vertical displacements is a Gaussian distribution fit given by

$$[1] \quad v = v_p \exp \left[ -\frac{1}{2} (x - x_0)^2 / i^2 \right]$$

where  $v_p$  is the peak vertical displacement,  $x_0$  is the horizontal offset of the peak from the centre line, and  $i$  is the trough width. This provides a very good fit ( $R^2 > 0.980$ ) to the measured data using the parameters given in Table 3. Now, the trough width parameters are very similar between the three tests, and this is further illustrated in Fig. 17 where the vertical displacements normalized by  $v_p$  are plotted against  $(x - x_0)$ . When normalized, differences between the three tests are not statistically significant at the 95% confidence interval. Thus, for all practical purposes, a trough width parameter of 0.5 m can be used to capture the measured displacements. This also suggests that the stiff trench had a significant impact on the measured surface displacements.

**Fig. 17.** Normalized vertical displacement. T1, T2, and T3, represent tests 1, 2, and 3, respectively.

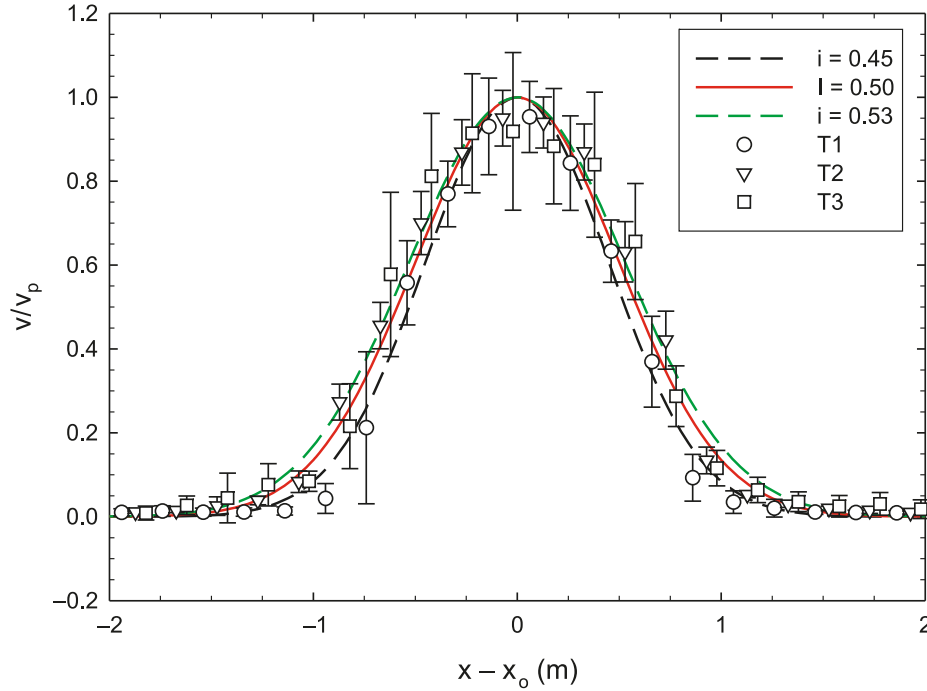


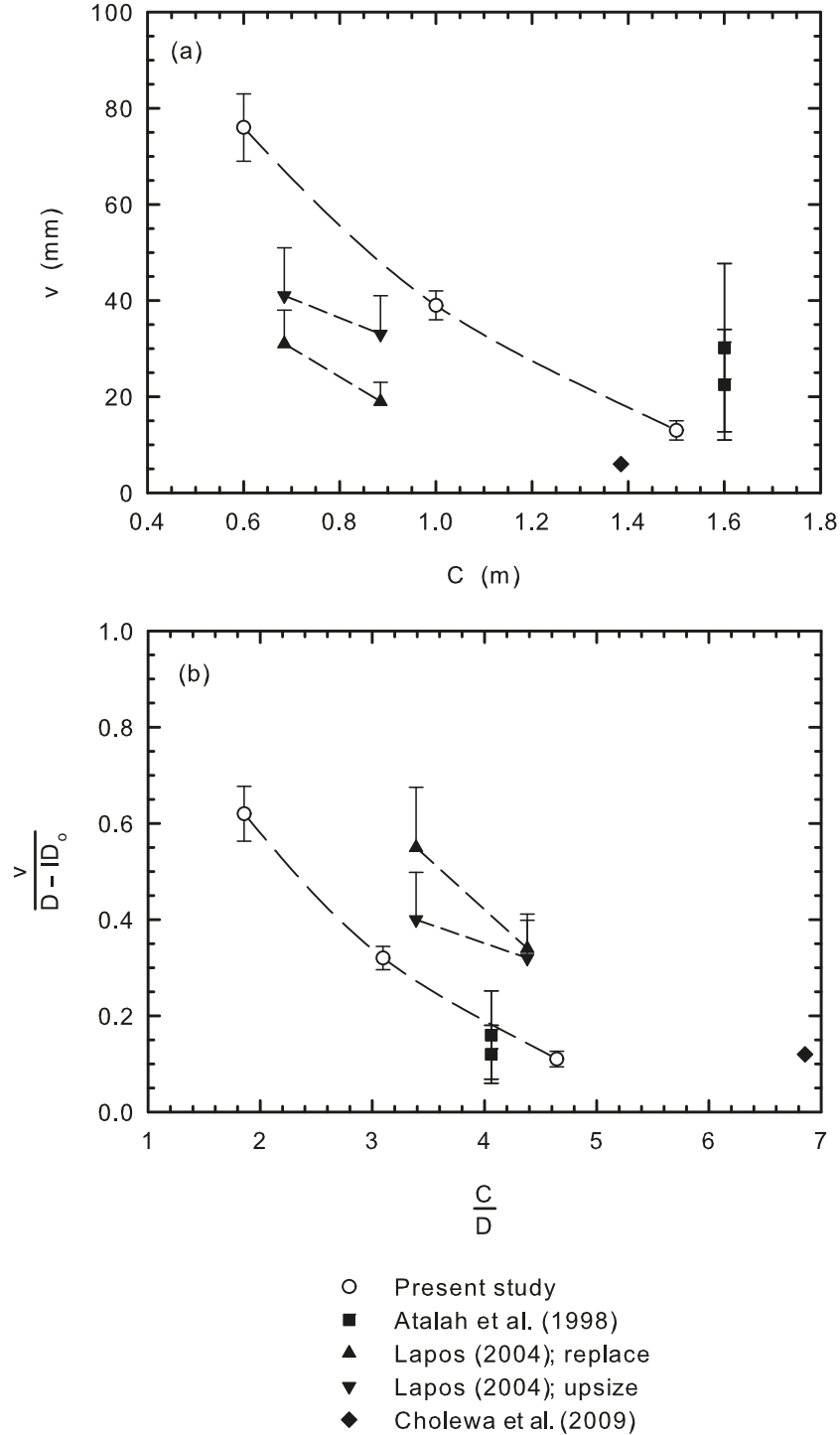
**Table 4.** Comparison of maximum vertical displacements.

Study	Condition	Backfill	Depth of cover, $C$ (m)	Original pipe inside dia., $ID_o$ (mm)	Expander dia., $D$ (mm)	$D - ID_o$ (mm)	Avg. $v$ (mm)	Max. $v$ (mm)
Atalah et al. (1998)	Recently back-filled trench in clay	Mixed clay and gravel to pipe crown then clay to surface	1.6	203	394	191	23	34
		Sand to pipe crown then clay to surface	1.6	203	394	191	30	48
Lapos (2004)	2 m wide trench with rigid walls	Poorly graded dense sand	0.7	146	202	56	31	38
			0.9	146	202	56	19	23
			0.7	100	202	102	41	51
Cholewa et al. (2009)	8 m wide embankment	Well-graded dense sand and gravel	0.9	100	202	102	33	41
			1.4	153	202	49	6	
Present study	0.8 to 1 m wide trench in stiff clay	Gravel to pipe crown then compacted clay to surface	0.6	200	323	123	76	83
			1.0	200	323	123	39	42
			1.5	200	323	123	13	15

The measured surface displacements are compared in Fig. 18 to previous studies involving static pipe bursting with no surface pavement layer. Atalah et al. (1998) reported results involving clay backfill in a trench, Lapos (2004) reported for poorly graded sand, and Cholewa et al. (2009) reported for well-graded sand and gravel. In addition

to different soil materials, the four studies involved different trench widths and different levels of upsizing (i.e.,  $D - ID_o$ ) as summarized in Table 4. Figure 18a plots the measurements of vertical surface displacement against the actual cover depth. The same values are also plotted in Fig. 18b, which shows the vertical displacement normalized by the

**Fig. 18.** Comparison of measured values with previously reported data.



difference between the largest diameter of the expander and the inside diameter of the original pipe,  $D - ID_0$ , versus the cover depth normalized by the diameter of the expander,  $C/D$ . For reference, if the expander remains concentric with the original pipe (i.e., their axes coincide), then the upward vertical displacement imposed at the crown of the original pipe is equal to  $0.5(D - ID_0)$ . The values of Atalah et al. (1998) are larger than those from the present study

cover ( $C = 1.6$  m versus  $C = 1.5$  m), as shown in Fig. 18a. This is because a larger expander was used by Atalah et al. (1998). The normalized results from the two studies involving clay are quite similar, as the results from Atalah et al. (1998) match the trend from the present work (Fig. 18b). It is unknown as to why the displacements reported by Atalah et al. (1998) are much more variable than those of this study for comparable  $C/D$  values.

Figure 18a also shows that conditions of the present study produced larger surface displacements than the sand results of Lapos (2004) at a comparable cover. This is entirely a result of the larger expander used in the present study. When normalized, the sand displacements are a much larger proportion of  $(D - ID_o)$  than those for clay. This is because much greater volume increases occurred upon shear failure (i.e., dilation) for the sand than for the clay considered in the present study, and the expander may also have ridden directly on the invert of the original pipe when buried in sand rather than clay.

Ground displacements would be expected to be greater than those measured if the expander size was increased relative to the original pipe that was tested (i.e., where pipe up-sizing occurred rather than replacement). The reported data from the present study are not intended to provide direct guidance on how displacements would change in this scenario, but rather are intended provide a database of well-documented surface displacement measurements that could be used to validate and calibrate numerical procedures (e.g., Nkemitag and Moore 2007) that would then permit predictions for other expander geometries or different ground conditions.

## Conclusions

Three-dimensional surface displacements from 20 m long static pipe-bursting experiments have been reported. These experiments were conducted with firm-to-stiff clay backfill in a trench with very stiff clay sidewalls at three different burial depths. Multiple digital cameras and image analysis were used to quantify the three-dimensional response of the ground surface as the expander progressed through the original pipe. For the specific conditions tested, it was concluded that

- (1) The upward ground surface movements reached peak values within 2 m of commencement of the bursting process at depths of 0.6 and 1 m, but took over 5 m to reach the peak for the pipe replaced at 1.5 m depth. Variability was measured that increased with shallower cover. The relative location of the burst head when the surface reached its maximum value ranged from just ahead to just behind the expander — depending on the burial depth.
- (2) The ground surface moved axially forward as the expander approached, increased to a maximum just ahead of the expander — with the distance away from the expander decreasing with increasing burial depth, and then decreased to have essentially no permanent residual axial displacement. The magnitude of the maximum axial ground movements was approximately 15%–20% of the maximum uplift.
- (3) The ground surface experienced horizontal displacements away from the centreline that were essentially zero at the centreline, increased to a maximum, and then decreased further away from the centreline. Axial surface cracks were observed for the two shallow burial depths tested, which were consistent with horizontal elongation of the ground surface above the original pipe. The magnitude of the maximum lateral ground

movements was approximately 13%–20% of the maximum uplift.

- (4) While the magnitude of the peak vertical surface displacement increased with decreasing burial depth (as expected), to all practical purposes, the three different burial depths produced the same width of vertical surface response with the displacements contained within  $\pm 1.5$  m of the centreline. The results suggest that the stiff clay trench walls had a dominant influence on the pattern of measured displacements.

## Acknowledgements

The research was funded by TT Technologies Inc. (Aurora, Ill., USA), the Premier's Research Excellence Award (awarded to R. Brachman), the Natural Sciences and Engineering Research Council of Canada, the Canada Foundation for Innovation, and the Ontario Innovation Trust. We appreciate the contributions of Kevin Nagle and Mark Maxwell from TT Technologies and Samuel Ariaratnam from Arizona State University in enabling the field work. The assistance provided by Jon Foster is also gratefully acknowledged.

## References

- Atalah, A., Sterling, R., Hadala, P., Akl, F., Lei, Y., and Du, X. 1998. The effect of pipe bursting on nearby utilities, pavement and structures. Trenchless Technology Center, Louisiana Tech University, Ruston, La. Technical Report No. TTC-98-01.
- Cholewa, J.A., Brachman, R.W.I., Moore, I.D., and Take, W.A. 2009. Ground displacements from a pipe-bursting experiment in well-graded sand and gravel. *Journal of Geotechnical and Geoenvironmental Engineering, ASCE*, **135**(11): 1713–1721. doi:10.1061/(ASCE)GT.1943-5606.0000117.
- Fernando, V. 2002. Mechanical response of HDPE pipe during pipe bursting. M.E.Sc. thesis, Faculty of Engineering Science, The University of Western Ontario, London, Ont.
- Lapos, B.M. 2004. Laboratory study of static pipe bursting three-dimensional ground displacements and pull force during installation, and subsequent response of HDPE replacement pipes under surcharge loading. M.Sc. thesis, Department of Civil Engineering, Queen's University, Kingston, Ont.
- McLeod, H.A. 2008. Field measurements of surface displacements from pipe bursting. M.Sc. thesis, Department of Civil Engineering, Queen's University, Kingston, Ont.
- Nkemitag, M., and Moore, I.D. 2007. Longitudinal progression of burst head during pipe bursting: calculation of pulling force. *Transportation Research Record*, **2028**: 203–210. doi:10.3141/2028-22.
- Rogers, C.D.F., and Chapman, D.N. 1995. An experimental study of pipebursting in sand. *Geotechnical Engineering. Proceedings - Institution of Civil Engineers*, **113**(1): 38–50.
- White, D.J., Take, W.A., and Bolton, M.D. 2003. Soil deformation measurement using particle image velocimetry (PIV) and photogrammetry. *Géotechnique*, **53**(7): 619–631.

## List of symbols

- $C$  depth of cover from outside of pipe crown to ground surface (L)  
 $D$  largest diameter of expander (L)  
 $ID_o$  inside diameter of original pipe (L)  
 $i$  trough width parameter (L)  
 $OD_f$  outside diameter of final pipe (L)

$q_c$	cone penetration test tip resistance ( $ML^{-1}T^{-2}$ )	$w_N$	natural gravimetric water content (%)
$R^2$	coefficient of determination	$w_p$	plastic limit (%)
$R_f$	cone penetration test friction ratio (%)	$x$	horizontal Cartesian coordinate (L)
$S_u$	undrained shear strength ( $ML^{-1}T^{-2}$ )	$x_o$	horizontal trough shift (L)
$u$	horizontal surface displacement (L)	$y$	vertical Cartesian coordinate (L)
$v$	vertical surface displacement (L)	$z$	axial Cartesian coordinate (L)
$v_p$	peak vertical surface displacement (L)	$z_B$	axial position of expander (L)
$v_{res}$	residual vertical surface displacement (L)	$\theta_v$	volumetric water content (%)
$w$	axial surface displacement (L)		
$w_L$	liquid limit (%)		